

Mueller matrix microscope: a quantitative tool to facilitate detections and fibrosis scorings of liver cirrhosis and cancer tissues

Ye Wang
Honghui He
Jintao Chang
Chao He
Shaoxiong Liu
Migao Li
Nan Zeng
Jian Wu
Hui Ma

Mueller matrix microscope: a quantitative tool to facilitate detections and fibrosis scorings of liver cirrhosis and cancer tissues

Ye Wang,^{a,b} Honghui He,^a Jintao Chang,^{a,b} Chao He,^{a,c} Shaoxiong Liu,^d Migao Li,^e Nan Zeng,^a Jian Wu,^a and Hui Ma^{a,b,*}

^aTsinghua University, Graduate School at Shenzhen, Institute of Optical Imaging and Sensing, Shenzhen Key Laboratory for Minimal Invasive Medical Technologies, 2279 Lishui Street, Shenzhen 518055, China

^bTsinghua University, Department of Physics, 1 Tsinghua Yuan, Beijing 100084, China

^cTsinghua University, Department of Biomedical Engineering, 1 Tsinghua Yuan, Beijing 100084, China

^dHuazhong University of Science and Technology Union Shenzhen Hospital, Shenzhen Sixth People's Hospital (Nanshan Hospital), 89 Taoyuan Street, Shenzhen 518052, China

^eGuangzhou Liss Optical Instrument Factory, 81 Taojinbei Street, Guangzhou 510095, China

Abstract. Today the increasing cancer incidence rate is becoming one of the biggest threats to human health. Among all types of cancers, liver cancer ranks in the top five in both frequency and mortality rate all over the world. During the development of liver cancer, fibrosis often evolves as part of a healing process in response to liver damage, resulting in cirrhosis of liver tissues. In a previous study, we applied the Mueller matrix microscope to pathological liver tissue samples and found that both the Mueller matrix polar decomposition (MMPD) and Mueller matrix transformation (MMT) parameters are closely related to the fibrous microstructures. In this paper, we take this one step further to quantitatively facilitate the fibrosis detections and scorings of pathological liver tissue samples in different stages from cirrhosis to cancer using the Mueller matrix microscope. The experimental results of MMPD and MMT parameters for the fibrotic liver tissue samples in different stages are measured and analyzed. We also conduct Monte Carlo simulations based on the sphere birefringence model to examine in detail the influence of structural changes in different fibrosis stages on the imaging parameters. Both the experimental and simulated results indicate that the polarized light microscope and transformed Mueller matrix parameters can provide additional quantitative information helpful for fibrosis detections and scorings of liver cirrhosis and cancers. Therefore, the polarized light microscope and transformed Mueller matrix parameters have a good application prospect in liver cancer diagnosis. © The Authors. Published by SPIE under a Creative Commons Attribution 3.0 Unported License. Distribution or reproduction of this work in whole or in part requires full attribution of the original publication, including its DOI. [DOI: [10.1117/1.JBO.21.7.071112](https://doi.org/10.1117/1.JBO.21.7.071112)]

Keywords: Mueller matrix; microscope; polarization; liver cancer; fibrosis.

Paper 150637SSRR received Sep. 28, 2015; accepted for publication Mar. 29, 2016; published online Apr. 18, 2016.

1 Introduction

As one of the most salient features of light, polarization can be used to develop imaging techniques capable of probing the structural and optical properties of media.^{1–3} Polarization imaging methods have the ability to measure the microstructural information nondestructively in tissues, cells, and other specimens.^{4,5} Polarization techniques can especially help suppress the multi-scattered photons from deep tissues, and thus improve the imaging contrast of superficial layers of samples.⁶ For this reason, in the past two decades, several techniques such as the degree of polarization and difference polarization have been applied to the detection of human skin cancers *in vivo*.^{7,8} Recently, as comprehensive descriptions of polarization properties, the Mueller matrix imaging techniques have been regarded as potential methods of cancerous tissues' diagnosis⁹ and preliminarily applied to the detection of colon cancer,^{10–12} thyroid cancer,¹³ cervical cancer,^{14,15} and so on.^{16–18} Through calculations using the Mueller matrix polar decomposition (MMPD) and Mueller matrix

transformation (MMT), groups of quantitative polarization imaging parameters with explicit physics meanings can be obtained.^{19,20}

Nowadays the increasing cancer incidence rate is becoming one of the biggest threats to human health. Among all types of cancers, liver cancer ranks in the top five in frequency with an estimated number of over 700,000 new cases a year all over the world. In high-risk countries including China, liver cancer can arise before the age of 20 years.^{21,22} According to the mortality rate in the United States, liver cancer will become the third leading cause of cancer-related death by 2030.²³ In China, there are over 350,000 new cases of liver cancer each year, accounting for more than 50% of those in the world.²⁴ During the development of liver hepatitis to cancer, fibrosis often evolves as part of a healing process in response to liver damage, resulting in cirrhosis of liver tissues.²⁵ The diagnosis of liver fibrosis is usually based on histological findings of liver biopsy observed by optical microscope.²⁶ This procedure needs stained tissue sections and experienced pathologists to result in accurate evaluations.²⁷ Recently, the second-harmonic generation (SHG) technique has been applied for quantitative assessment of fibrosis in chronic hepatitis B patients.²⁸ The results and analysis have shown

*Address all correspondence to: Hui Ma, E-mail: mahui@tsinghua.edu.cn

that the fibrosis scoring accuracy can be improved by SHG images and imaging processing methods. On the other hand, as an optical technique with simple structure and low cost, the polarization imaging can also be suitable for the detection of fibrous structures. Compared with the traditional optical microscope and SHG imaging, the Mueller matrix microscope and transformed parameters such as MMPD and MMT may provide more information on unstained fibrous structures whose orders of alignment are not so good. Therefore, the transformed Mueller matrix parameters can possibly be used as good indicators for pathological diagnosis of liver cancer. Recently, in order to extract microstructural information of pathological tissue slices more effectively, we designed a Mueller matrix microscope by adding both the polarization states generator and analyzer (PSG and PSA) to an ordinary commercial optical microscope.²⁵

In this paper, based on the methods proposed in a previous study,²⁵ we take it one step further to quantitatively facilitate the fibrosis detection and scorings of pathological liver tissue samples in different stages from cirrhosis to cancer using the Mueller matrix microscope. We measure and analyze the MMPD and MMT parameters for the fibrotic liver tissue samples in different stages. Then we conduct the Monte Carlo (MC) simulations based on the sphere birefringence model to examine in detail the influence of structural changes in different fibrosis stages on the imaging parameters. Both the experimental and MC simulated results indicate that the polarized light microscope and transformed Mueller matrix parameters have a good application prospect in liver cancer diagnosis and scoring.

2 Methods and Materials

2.1 Experimental Setup

Figure 1 shows the polarization Mueller matrix microscope used in this study. The microscope was transformed from a commercial transmission microscope (Yuexian L2050, Guangzhou, China) by adding the PSG and PSA. The light source is an LED (3 W, 632 nm, $\Delta\lambda = 20$ nm). The polarization states of the incident light are controlled by the PSG consisting of a set of a linear polarizer (P1, extinction ratio 500:1, Daheng Optics, China) and a quarter-wave plate (R1, Daheng Optics). The polarized light passes through the tissue sample on the stage and the objective lens, and then the PSA, consisting of another set of a quarter-wave plate (R2, Daheng Optics) and a linear polarizer (P2, extinction ratio 500:1, Daheng Optics). Both the PSG and PSA have been designed to be compact modules, as shown in Fig. 1, to be incorporated into the microscope. The emitted light is collected by a 12-bit CCD camera (QImaging 74-0107A, Canada) to produce the polarization images of the sample. For the Mueller matrix measurement, 30 images with specific incident and output polarization states are obtained. Using 30 images, we can estimate the Fourier coefficients needed to compute the Mueller matrix elements.

During the experiments, the polarizers (P1 and P2) are fixed in the 0-deg direction. The two quarter-wave plates (R1 and R2) are rotated harmonically to generate the polarized light. In addition, the rotation rates of the quarter-wave plates R1 and R2 are $\omega_2 = 5\omega_1$. Therefore, the intensity of light can be given by the following equation:

$$I_{\text{out}} = a_0 + \sum_{n=1}^{12} (a_n \cos n\omega t + b_n \sin n\omega t), \quad (1)$$

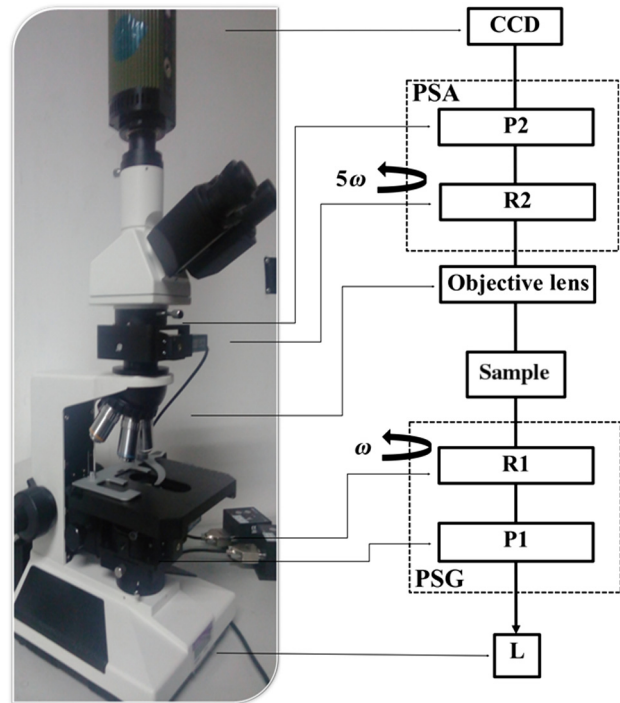


Fig. 1 Schematics of the polarized light microscope. P: polarizer; R: quarter-wave plate; L: light source; PSG: polarization states generator; and PSA: polarization states analyzer.

where a_n and b_n are the Fourier coefficients, and ω is the rotating angular speed of R1. The Mueller matrix elements can be calculated using the Fourier coefficients according to Ref. 29. More details for this Mueller matrix imaging method can be found in Refs. 30 and 31. To calibrate the microscope, we measured some standard samples including air, a quarter-wave plate, and a polarizer. We compensated the errors due to nonideal quarter-wave plates and polarizers as described in Ref. 32. The experimental results testified that the maximum errors for the absolute values of the Mueller matrix elements are about 0.01.

2.2 Mueller Matrix Polar Decomposition and Mueller Matrix Transformation Parameters

Mueller matrices contain abundant structural and optical information of samples. However, since the Mueller matrix elements lack clear physics meanings and relations to certain microstructures, there are huge difficulties in applying Mueller matrix polarimetry to biomedical studies, especially for quantitative analysis. Recently, several approaches to transform Mueller matrix elements to quantitative parameters with explicit physics meanings have been proposed. In this paper, we adopt the parameters of both MMPD and MMT techniques to analyze the microscopic imaging results of the liver tissue samples. The MMPD method is developed by Lu and Chipman¹⁹ and has been widely applied to biomedical studies.¹⁴⁻¹⁸ It is based on the three main interactions between the polarized light and media: diattenuation (D), retardation (δ), and depolarization (Δ). In MMPD, a Mueller matrix (M) can be decomposed and the linear retardance (δ) and its orientation angle (θ) can be derived by the following equations:

$$\begin{aligned}
 M &= M_{\Delta} M_R M_D \\
 \delta &= \cos^{-1}(\{[M_R(2,2) + M_R(3,3)]^2 \\
 &\quad + [M_R(3,2) + M_R(2,3)]^2\}^{1/2}) \\
 \theta &= 0.5 \tan^{-1}(r_2/r_1), \quad (2)
 \end{aligned}$$

where r_1 and r_2 are the elements of the retardance vector, and M_R is the sub-matrix of retardance.³³

In previous studies, by fitting the Mueller matrix elements into certain trigonometric functions, we proposed the MMT method. The MMT method can provide a set of parameters which is insensitive to the azimuth angle for the backscattering imaging of bulk tissues²⁰ or transmission imaging of thin tissues with limited scattering such as the pathological sections of liver tissues used in this paper.²⁵ Therefore, the MMT parameters t and x suitable for transmission microscopic imaging can be acquired by the following equations:

$$t = \frac{\sqrt{(m42)^2 + (m34)^2}}{2} \quad \tan(2x) = \frac{m42}{m34}. \quad (3)$$

Experiments and simulations have shown that the MMT parameter t and MMPD parameter δ are good indicators of the retardance of the media, while the MMT parameter x and MMPD parameter θ are related to the orientation directions of the aligned fibrous structures.^{25,34–36} The MMPD parameters are slightly more sensitive to the fibers, whereas the MMT parameters can be calculated more easily and quickly.³⁷ In our recent studies, we have found that, for the thin tissue slices with anisotropic fibrous structures, the birefringence effect plays the dominant role for the polarization imaging contrast mechanism;³⁷ therefore, for the cancerous liver tissue sections, the values of parameters δ and t and the distribution of parameters θ and x may be used to reflect the density and orientation of the fibrous structure.

2.3 Liver Tissue Samples

Polarization techniques can effectively improve the imaging quality and contrast of superficial tissues. Since most cancers occur in the superficial epithelium throughout the body in the early stage,³⁸ polarization imaging techniques have been regarded as potential methods of cancerous tissues diagnosis. In recent studies, we have found that the cancerous liver tissues contain abundant fibrous structures, which can be detected by polarization parameters.²⁵ In this study, we choose some human liver cirrhosis and cancer tissues with fibrosis as the samples for the polarized Mueller matrix microscope. As shown in Fig. 2, the samples are nonstained, dewaxing sections of pathological liver tissue slices, which are prepared and provided by Shenzhen Sixth People's (Nanshan) Hospital. For the liver cancer tissues, there are always inflammatory reactions accompanied by fibrosis formations. In addition, the pathological liver tissues of different stages have different proportions of fibrous structures, which can be used as the indicators for stage scorings.³⁹ We choose four 8- μm -thick slices of human liver tissues in different fibrosis stages (F1 to F4) as the imaging samples, as shown in Figs. 2(a)–2(d). For comparisons, the corresponding 4- μm -thick hematoxylin–eosin (H–E) stained slices shown as Figs. 3(a)–3(d) are also provided. This work was approved by the Ethics Committee of the Shenzhen Sixth People's (Nanshan) Hospital.

3 Results and Discussion

3.1 Microscopic Imaging Results of Liver Tissue Samples

Figure 2(a) shows the intensity image of the 8- μm -thick nonstained slice of the liver tissue with fibrosis in F1 stage under 4 \times objective observation. Figures 4(a)–4(d) are the images of the MMPD and MMT parameters δ , t , θ , and x . Previous studies have shown that δ and t are related to the

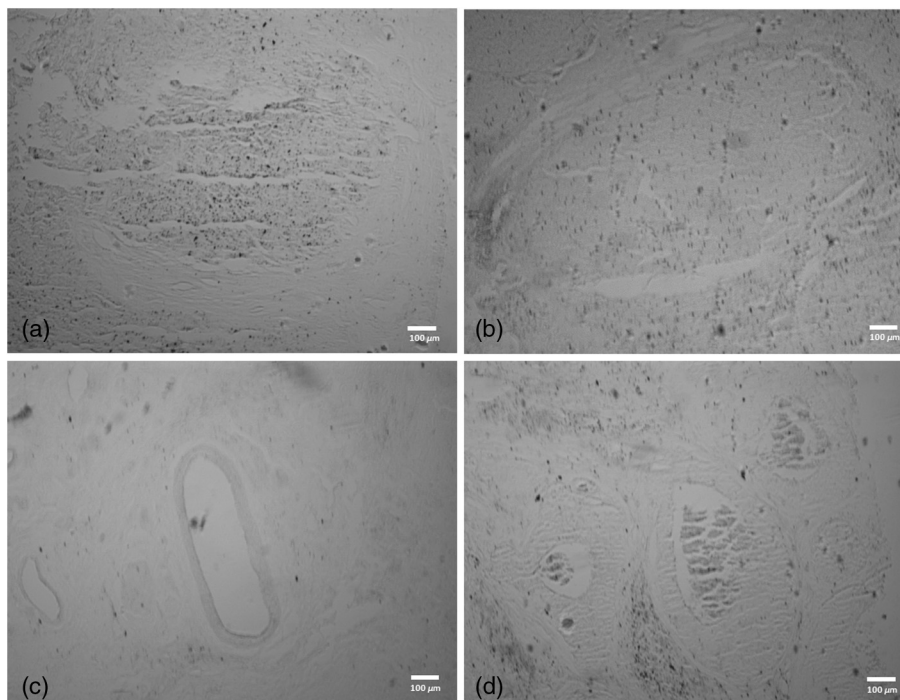


Fig. 2 Microscopic intensity images of the 8- μm -thick nonstained dewaxing slices of liver tissues with fibrosis in different pathological stages: (a) F1, (b) F2, (c) F3, and (d) F4.

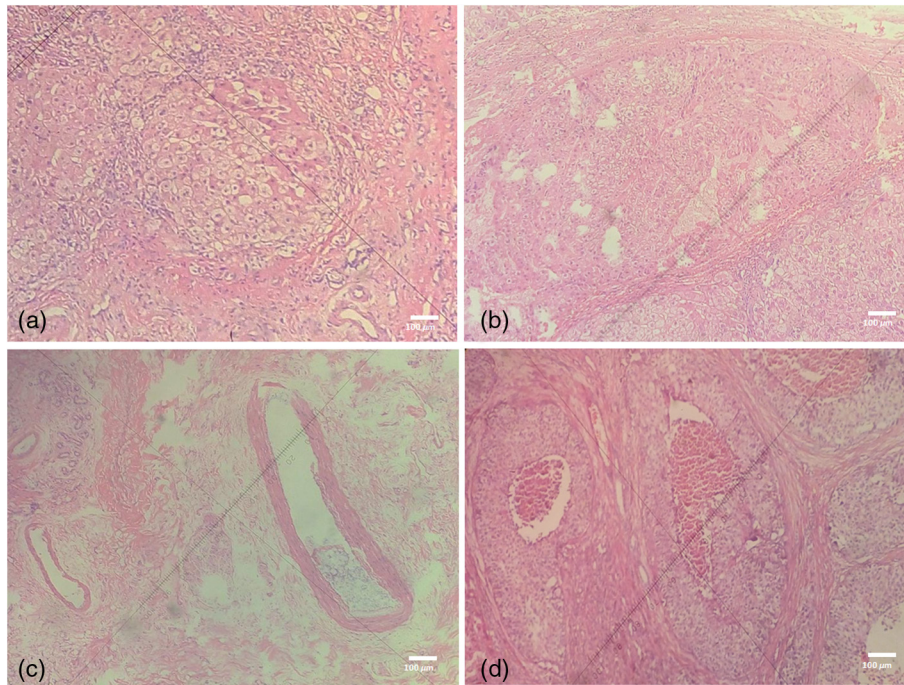


Fig. 3 Microscopic images of the corresponding H-E stained slices of human liver tissues with fibrosis in different pathological stages: (a) F1, (b) F2, (c) F3, and (d) F4.

retardance and θ and x are related to the angle orientation of the fibrous structures. From the intensity image shown as Fig. 2(a), the fibrous structures around the liver cells can hardly be discriminated. However, from the images of the parameters δ and t shown in Fig. 4, we can see that there are blurred circular

regions with relatively high values, indicating the existence of fibers. As mentioned above, the fibrosis process is closely related to the inflammatory reaction. It can be observed from Figs. 4(a) and 4(b) that the values of parameters δ and t for the fibrotic circular regions are larger than the other parts,

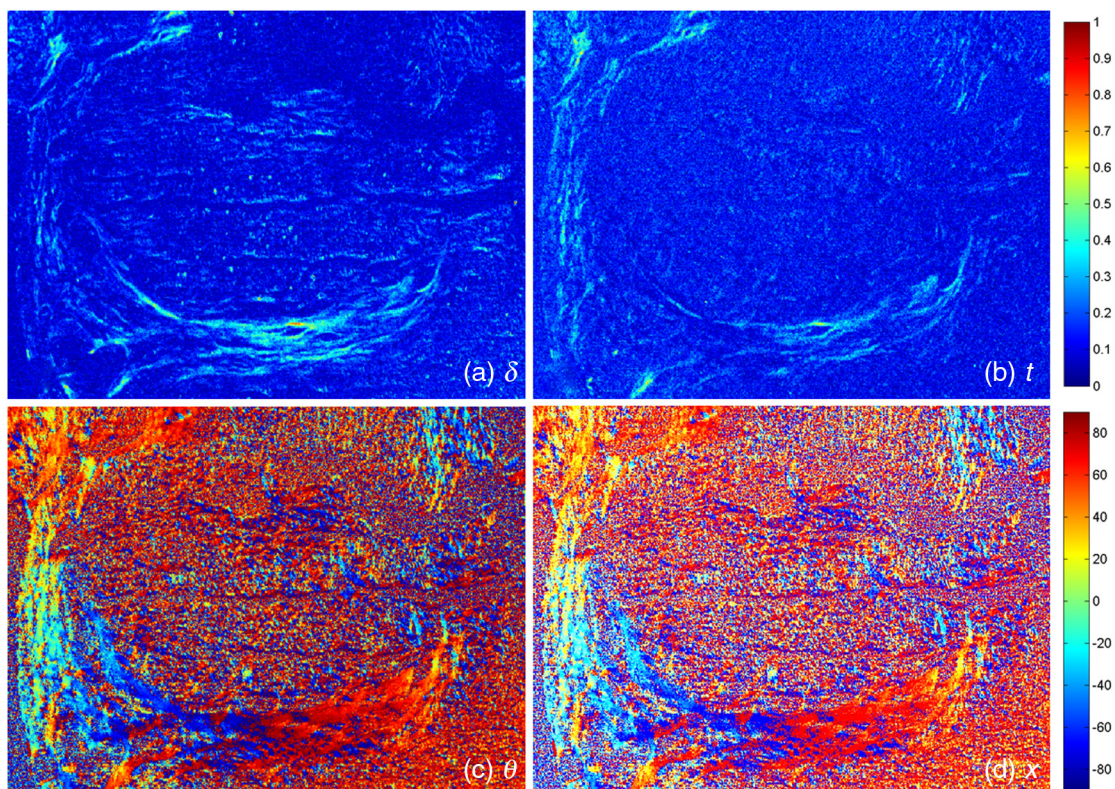


Fig. 4 Images of the 8- μ m-thick nonstained dewaxing slice of liver tissue with fibrosis in F1 stage: (a) MMPD δ , (b) MMT t , (c) MMPD θ , and (d) MMT x .

which means that the liver tissues with fibrosis have more prominent retardance than the normal tissues. Moreover, we can see that the lower right regions have the largest values of δ and t , indicating the densest fibers are distributed here. By implementing the image analysis and processing method used by Dubreuil et al.,³⁹ it is found that the largest values of parameters δ and t of the entire image are 0.41 and 0.38, respectively, and the proportion of fibrous distribution is about 6%. In addition to the density, from the images of the parameters θ and x shown as Figs. 4(c) and 4(d), the alignment orientations of the circular aligned fibers can be roughly revealed. The microscopic imaging results indicate that in F1 stage there are fibers existing in the liver tissues, but the fibrosis is not particularly evident, which is in accordance with the pathological description.

For comparisons, we then apply the Mueller matrix microscopy to the liver tissue with fibrosis in the F2 stage, whose intensity image under 4 \times objective observation is shown as Fig. 2(b). Figures 5(a)–5(d) are the images of the MMPD and MMT parameters δ , t , θ , and x . Some circularly aligned fibrous structures around the liver cells can be vaguely seen in Fig. 2(b). Figures 5(a) and 5(b) confirm that the values of parameters δ and t for the fibrotic circular regions are larger than the other parts, and the lower right regions have the largest values, meaning that the fibrosis degree of these regions is probably more obvious. We also notice that compared with the liver tissue in the F1 stage, the retardance of the sample in the F2 stage can be more prominent. Calculations show that the largest values of parameters δ and t of the entire image are 0.78 and 0.75, respectively, and the proportion of fibrous distribution is about 10%. From the images of the parameters θ and x shown as Figs. 5(c) and 5(d), the orientations of the fibrous

structures can be observed: the structural alignments for the upper left and lower right fibrotic regions are much clearer than the other parts. The results indicate that in the F2 stage the fibrosis in liver tissue becomes evident in some parts, which can also be observed in the pathological H–E stained section.

Figure 2(c) shows the intensity image of the liver tissue with cirrhosis in F3 stage under 4 \times objective observation. Figures 6(a)–6(d) are the images of the MMPD and MMT parameters δ , t , θ , and x . We can clearly see that there are some circularly distributed fibers in Fig. 2(c). The imaging results shown in Figs. 6(a) and 6(b) demonstrate that the parameters δ and t for the fibrotic circular regions have larger values than the other parts, indicating the existence of well-ordered fibers. In addition, there are some regions with relatively lower values surrounding the circular regions, meaning that the distribution range of fibrosis in the F3 stage may become wider than those in the F1 and F2 stages. Calculations show that the largest values of parameters δ and t of the entire image are 0.82 and 0.80, respectively, and the proportion of fibrous distribution is about 12%. It can also be observed from the images of parameters θ and x shown as Figs. 6(c) and 6(d) that the circularly aligned fibrotic regions have very clear distribution orientations. The results shown in Fig. 6 indicate that compared with the F1 and F2 stages, in the F3 stage the fibers in liver tissues are with a wider distribution and the fibrosis becomes more obvious in some regions.

Finally, we choose the 8- μ m-thick nonstained slice of cancerous liver tissue in the F4 stage, whose intensity image under 4 \times objective observation is shown as Fig. 2(d). In both the unstained Fig. 2(d) and H–E stained Fig. 3(d), we can see that there are abundant fibrous structures around the liver

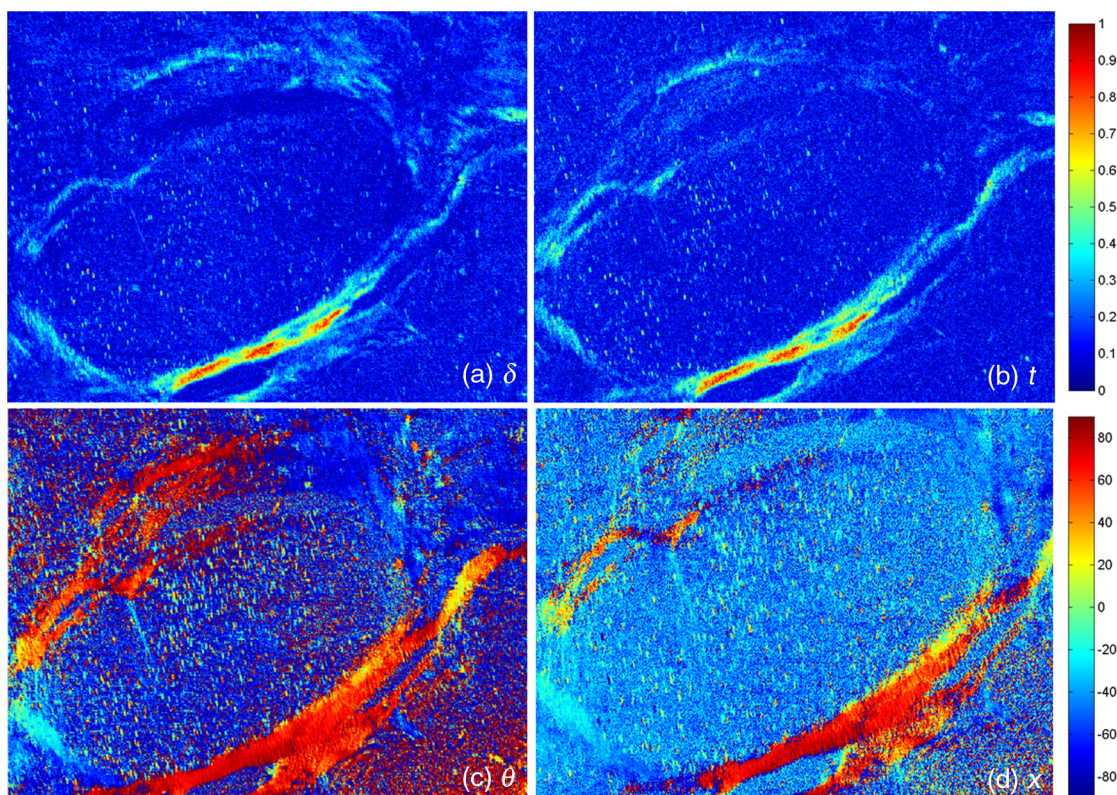


Fig. 5 Images of the 8- μ m-thick nonstained dewaxing slice of liver tissue with fibrosis in F2 stage: (a) MMPD δ , (b) MMT t , (c) MMPD θ , and (d) MMT x .

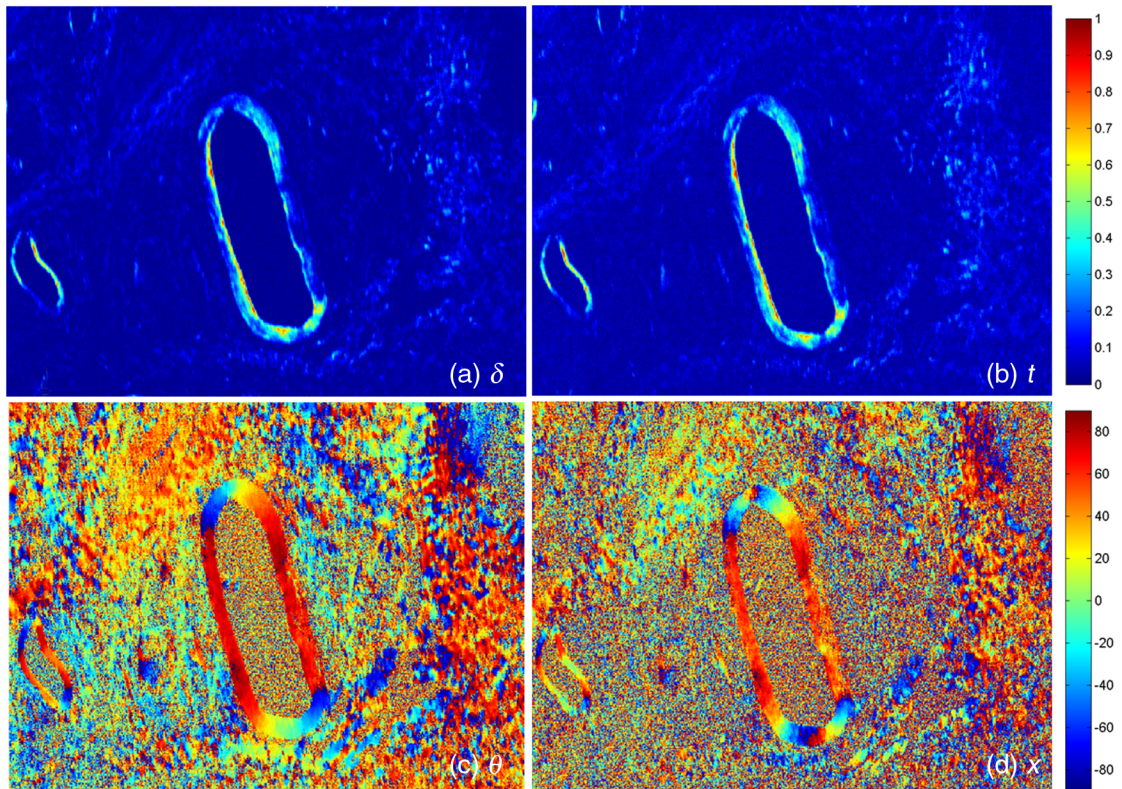


Fig. 6 Images of the 8- μm -thick nonstained dewaxing slice of liver cirrhosis tissue in F3 stage: (a) MMPD δ , (b) MMT t , (c) MMPD θ , and (d) MMT x .

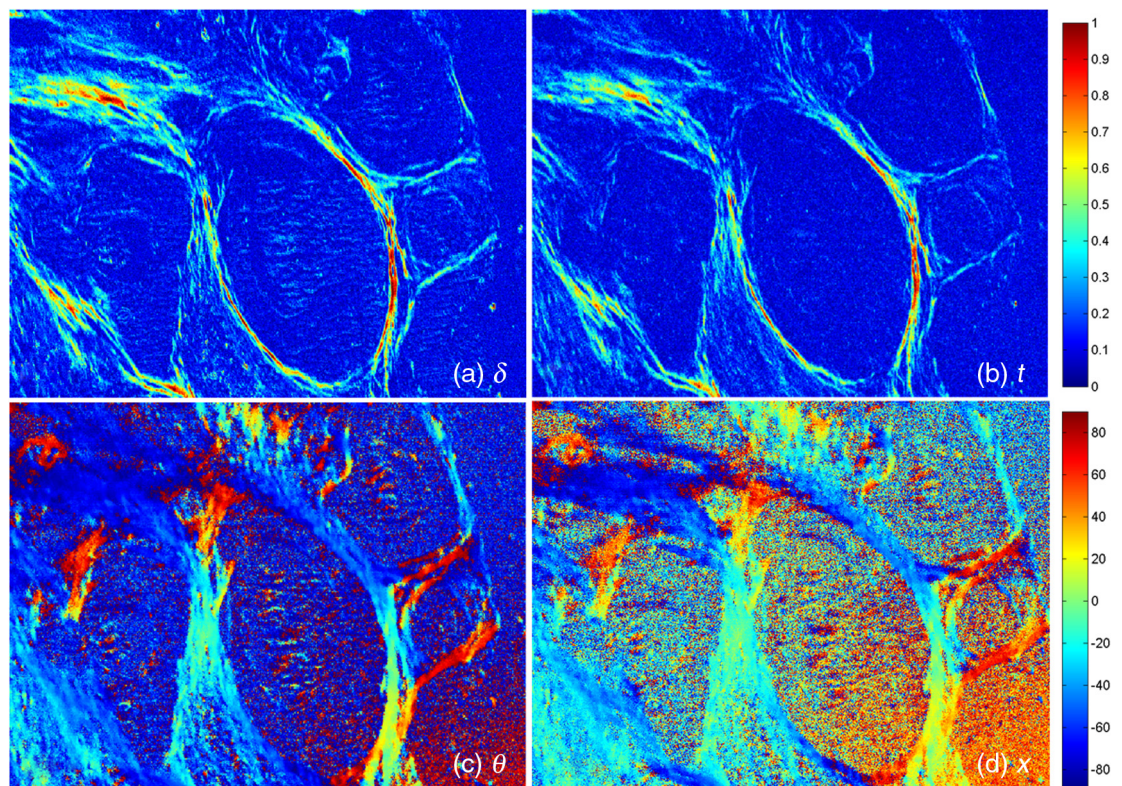


Fig. 7 Images of the 8- μm thick nonstained dewaxing slice of cancerous liver tissue with fibrosis in F4 stage: (a) MMPD δ , (b) MMT t , (c) MMPD θ , and (d) MMT x .

cells. Figures 7(a) and 7(b) show that the values of parameters δ and t for the cancerous liver sample are much larger than the samples in the F1 to F3 stages. Moreover, the boundaries of the fibrotic regions are clear, demonstrating that the fibrosis degree of these regions is very high. Calculations show that the largest values of parameters δ and t of the entire image are 0.96 and 0.95, respectively, and the proportion of fibrous distribution is about 16%. The images of parameters θ and x shown as Figs. 7(c) and 7(d) also reveal that there are a large portion of fibers with distinct orientations in the cancerous liver tissue. The results shown in Figs. 4–7 testify that: (a) both the microscopic MMPD and MMT parameters can be used as the potential indicators for the fibrosis process in pathological liver tissue samples. (b) As the development of cancer-induced inflammatory reaction increases, the proportion of fibrous structures in liver tissues becomes larger. In the F4 stage, the fibers are much denser than in the F1 to F3 stages, which can be clearly observed using the Mueller matrix microscope.

3.2 Quantitative Analysis of Imaging Results

For a more detailed analysis of the characteristic variations of parameters δ , t , θ , and x in different stages, we make quantitative studies in this section. First, from Fig. 8, which shows the average values over the entire images of the parameters δ and t in different fibrosis stages, we can see that both the parameters increase as the stage changes from F1 to F4. This is because a higher development stage means a larger amount of fibers in the liver tissues, leading to a more prominent retardance effect. In addition, it is also shown that from F1 to F4, the mean value of parameter δ changes more prominently than that of parameter t , indicating that parameter δ may be more sensitive to the variations of fibrous structures. Although more statistical studies are still needed, the preliminary results demonstrate that the parameters δ and t may be used as quantitative tools for the detection and scorings of liver cirrhosis and cancer. Second, from Fig. 9, which shows the distribution histograms of the parameter θ in different stages, we can see that: (a) The values of parameter θ have a relatively uniform distribution in the F1 stage. (b) The distribution of the parameter θ begins to converge to certain values in the F2 and F3 stages. (c) In the F4 stage, the convergence of parameter θ becomes prominent, showing abundant fibrous structures distributed in a relatively narrow range of

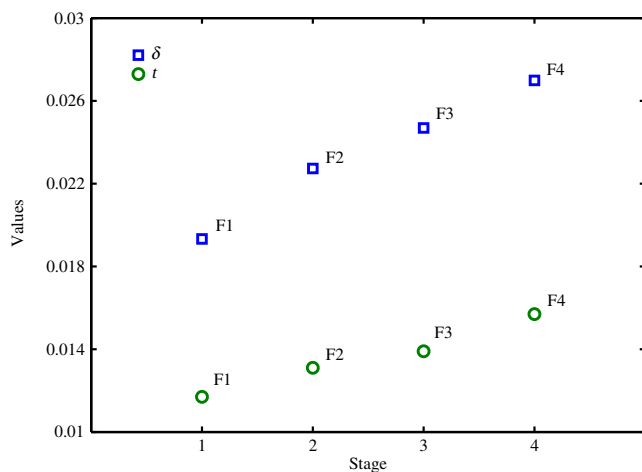


Fig. 8 Average experimental values of parameters δ (blue squares) and t (green circles) in different stages.

orientations. The characteristic distribution feature of parameter x is very similar to parameter θ . The results shown in Fig. 9 indicate that, although more statistical analyses are still needed, the distribution feature of the parameter θ or x may offer information to help determine the fibrosis degree. Since the pathological liver tissues in different stages have different proportions of fibrous microstructures, the results shown in Figs. 8 and 9 confirm that the MMPD and MMT parameters can provide additional quantitative information helpful for the accurate fibrosis scorings of liver cirrhosis and cancers.

In order to interpret the experimental results above, we carry on MC simulations based on the sphere birefringence model to analyze the relationship between the parameters and the fibrosis process of the liver tissues.⁴⁰ In the MC simulations, there are two types of spherical scatterers, the large ones ($8 \mu\text{m}$ in diameter, scattering coefficient is 150 cm^{-1}) represent the cell nuclei and the small ones ($0.5 \mu\text{m}$ in diameter, scattering coefficient is 50 cm^{-1}) represent the organelles. According to the liver tissue samples, the thickness of the medium is $8 \mu\text{m}$ and the refractive indices of the interstitial medium and scatterers are 1.33 and 1.45, respectively.³⁷ As mentioned in Sec. 2.2, for the thin tissue slices with anisotropic fibrous structures, the birefringence effect plays the dominant role for the polarization imaging contrast mechanism.³⁷ In addition, the experimental results have shown that from stage F1 to F4 not only the values of retardance of fibrotic regions, but also the proportion of fibrous distribution increase. Therefore, to quantitatively analyze the fibrosis process during the F1 to F4 stages, in the MC simulations, both the increases of birefringence value Δn and proportion of fibrous distribution are considered. As shown in Fig. 10, in the simulations, the value of Δn is increased from 0.001 to 0.0025 and the optical axis is along the x -axis direction. Meanwhile, the proportion of fibrous distribution is changed from 6%, 10%, 12%, to 16% according to the experimental results. The simulated results shown in Fig. 10 demonstrate that the values of parameters δ and t increase as the birefringence increases, which are consistent with the experimental observations. It should be pointed out that in Fig. 10, the absolute values of the parameters δ and t are slightly lower than those in Fig. 8. In the MC simulation, there are several constant parameters used such as the thickness of the medium and the diameter of the scatterers. Actually, these parameters can be varied in different regions of the tissue samples. Since such variations are hard to estimate, we use approximately constant values of these parameters, which may influence the results of the MC simulations. It can also be observed that when Δn changes from 0.001 to 0.0025, the mean value of parameter δ changes about 0.02, while the mean value of parameter t changes only about 0.01, meaning that the MMPD parameter δ is slightly more sensitive to the variations of Δn . Figure 11 shows that both the parameters θ and x can reflect the orientation of the optical axis or the alignment direction of the fibers. It should be pointed out that in MC simulations, when the value of Δn is changed from 0.001 to 0.0025, or the proportion of fibrous distribution is changed from 6% to 16%, the curves shown in Fig. 11 almost remain the same, confirming that the parameters θ and x are insensitive to the value of Δn .

In summary, the experimental and MC simulated results demonstrate that the polarization Mueller matrix microscope can provide quantitative information of the pathological changes of liver tissues in different fibrosis stages. During the development of liver hepatitis and cancers, the inflammatory reactions

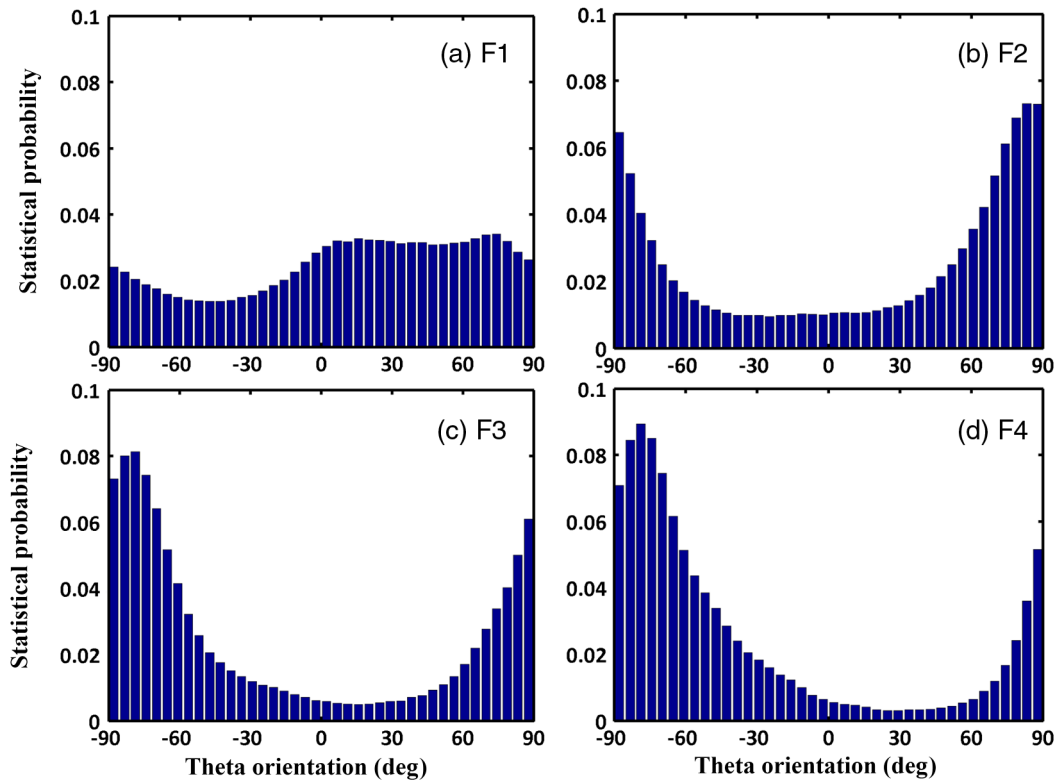


Fig. 9 Statistical distribution histograms of the experimental results for parameter θ in different stages.

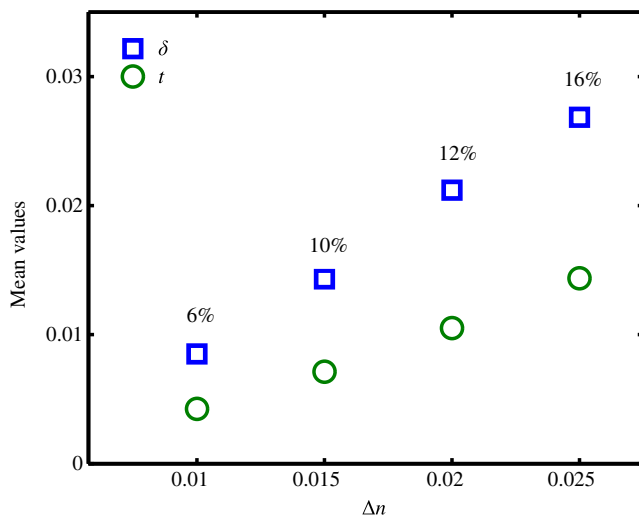


Fig. 10 MC simulated results of the parameters δ (blue squares) and t (green circles) using the sphere birefringence model. The value of birefringence Δn changes from 0.001 to 0.0025. The proportion of fibrous distribution changes from 6% to 16% as indicated in the image.

can result in fibrosis and cirrhosis, which can be reflected by the values of the MMPD and MMT parameters. Although both the MMPD and MMT methods can be used for the detection of fibrous microstructures, they have different advantages: the MMPD parameters are slightly more sensitive to the fibers, whereas the MMT parameters are easier and quicker to compute.³⁷ In this study, when a Mueller matrix is known, the calculation time of MMT parameters is 0.02 s, while the calculation time of MMPD parameters is 60.22 s with Intel(R) Core

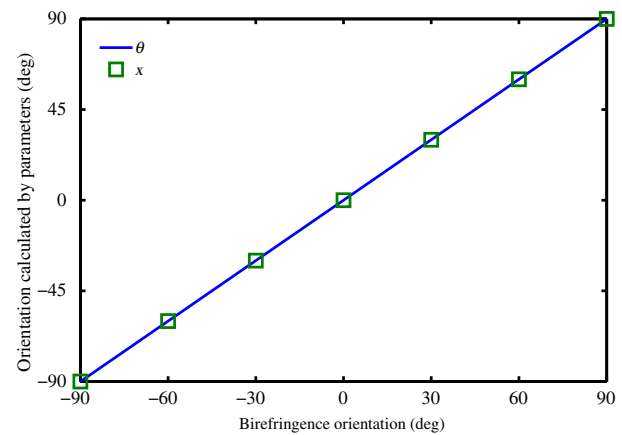


Fig. 11 MC simulated results of the parameters θ (blue line) and x (green squares) using the sphere birefringence model. The orientation of the birefringence changes from -90 deg to 90 deg. The value of birefringence Δn is 0.001. The proportion of fibrous distribution is 6%.

(TM) i7-3770 CPU and MATLAB 2014. It is shown that the Mueller matrix microscope and transformed parameters can be applied as potential tools to liver cancer stage scoring.

4 Conclusion

In this paper, we apply the Mueller matrix microscope to pathological liver cirrhosis and cancer tissue samples in the F1 to F4 fibrosis stages. We also adopt both the MMPD and MMT parameters for the quantitative analysis of the liver tissues. The microscopic imaging results demonstrate that the parameters δ , t , θ , and x can be used as tools for the detection of fibrous

liver tissues. Since the pathological liver tissues in different stages have different proportions of fibrous microstructures, the experimental results show that the MMPD and MMT parameters can provide additional quantitative information helpful for the fibrosis detection and accurate scorings of liver cirrhosis and cancers. We conduct MC simulations based on the sphere birefringence model to analyze the relationship between the parameters and the fibrosis process of the liver tissues. Both the experimental and MC simulated results indicate that the polarized light microscope and transformed Mueller matrix parameters have a good application prospect in liver cancer diagnosis. In addition, through some more comprehensive transformation process of the Mueller matrix elements, we may obtain more quantitative parameters for the extraction of the intrinsic microstructural characteristic features of liver cancerous tissues. In future studies, statistical analysis of more fibrotic liver tissue samples is still needed to establish reliable relationship between the pathological structural features and the polarization imaging parameters. Also, analyzing methods such as the central moment parameters can be adopted to extract more quantitative indicators to facilitate fibrosis detections and scorings of liver cirrhosis and cancer tissues.

Acknowledgments

This work has been supported by National Natural Science Foundation of China (NSFC) (Grant Nos. 11174178, 11374179, 61205199, and 61405102) and Science and Technology Project of Shenzhen (Grant Nos. CXZZ20140509172959978 and GJHZ20150316160614844).

References

- N. Ghosh and I. A. Vitkin, "Tissue polarimetry: concepts, challenges, applications, and outlook," *J. Biomed. Opt.* **16**(11), 110801 (2011).
- R. Oldenbourg, "A new view on polarization microscopy," *Nature* **381**(6585), 811–812 (1996).
- N. T. Clancy et al., "Polarised stereo endoscope and narrowband detection for minimal access surgery," *Biomed. Opt. Express* **5**(12), 4108–4117 (2014).
- B. Kunnen et al., "Application of circularly polarized light for non-invasive diagnosis of cancerous tissues and turbid tissue-like scattering media," *J. Biophotonics* **8**(4), 317–323 (2015).
- L. Liu et al., "A reliable, noninvasive technique for spindle imaging and enucleation of mammalian oocytes," *Nat. Biotechnol.* **18**(2), 223–225 (2000).
- R. S. Gurjar et al., "Imaging human epithelial properties with polarized light-scattering spectroscopy," *Nat. Med.* **7**(11), 1245–1248 (2001).
- S. L. Jacques, J. C. Ramella-Roman, and K. Lee, "Imaging skin pathology with polarized light," *J. Biomed. Opt.* **7**(3), 329–340 (2002).
- R. R. Anderson, "Polarized light examination and photography of the skin," *Arch. Dermatol.* **127**(7), 1000–1005 (1991).
- S. Alali and I. A. Vitkin, "Polarized light imaging in biomedicine: emerging Mueller matrix methodologies for bulk tissue assessment," *J. Biomed. Opt.* **20**(6), 061104 (2015).
- A. Pierangelo et al., "Multispectral Mueller polarimetric imaging detecting residual cancer and cancer regression after neoadjuvant treatment for colorectal carcinomas," *J. Biomed. Opt.* **18**(4), 046014 (2013).
- I. Ahmad et al., "Ex vivo characterization of normal and adenocarcinoma colon samples by Mueller matrix polarimetry," *J. Biomed. Opt.* **20**(5), 056012 (2015).
- A. Pierangelo et al., "Ex-vivo characterization of human colon cancer by Mueller polarimetric imaging," *Opt. Express* **19**(2), 1582–1593 (2011).
- H. He et al., "Mapping local orientation of aligned fibrous scatterers for cancerous tissues using backscattering Mueller matrix imaging," *J. Biomed. Opt.* **19**(10), 106007 (2014).
- A. Pierangelo et al., "Polarimetric imaging of uterine cervix: a case study," *Opt. Express* **21**(12), 14120–14130 (2013).
- P. Shukla and A. Pradhan, "Mueller decomposition images for cervical tissue: potential for discriminating normal and dysplastic states," *Opt. Express* **17**(3), 1600–1609 (2009).
- J. Jagtap et al., "Quantitative Mueller matrix fluorescence spectroscopy for precancer detection," *Opt. Lett.* **39**(2), 243–246 (2014).
- W. Wang et al., "Roles of linear and circular polarization properties and effect of wavelength choice on differentiation between ex vivo normal and cancerous gastric samples," *J. Biomed. Opt.* **19**(4), 046020 (2014).
- J. Chung et al., "Use of polar decomposition for the diagnosis of oral precancer," *Appl. Opt.* **46**(15), 3038–3045 (2007).
- S. Y. Lu and R. A. Chipman, "Interpretation of Mueller matrix based on polar decomposition," *J. Opt. Soc. Am. A* **13**(5), 1106–1113 (1996).
- H. He et al., "A possible quantitative Mueller matrix transformation technique for anisotropic scattering media," *Photonics Lasers Med.* **2**(2), 129–137 (2013).
- F. X. Bosch et al., "Primary liver cancer: worldwide incidence and trends," *J. Gastroenterol.* **127**(5), S5–S16 (2004).
- F. X. Bosch, J. Ribes, and J. Borràs, "Epidemiology of primary liver cancer," *Semin. Liver Dis.* **19**(3), 271–285 (1998).
- L. Rahib et al., "Projecting cancer incidence and deaths to 2030: the unexpected burden of thyroid, liver, and pancreas cancers in the United States," *Cancer Res.* **74**(11), 2913–2921 (2014).
- W. Chen et al., "Report of cancer incidence and mortality in China, 2010," *Ann. Transl. Med.* **2**(7), 61 (2014).
- Y. Wang et al., "Differentiating characteristic microstructural features of cancerous tissues using Mueller matrix microscope," *Micron* **79**, 8–15 (2015).
- D. B. Strader et al., "Diagnosis, management, and treatment of hepatitis C," *Hepatology* **39**(4), 1147–1171 (2004).
- P. Bedossa, D. Dargere, and V. Paradis, "Sampling variability of liver fibrosis in chronic hepatitis C," *Hepatology* **38**(6), 1449–1457 (2003).
- S. Xu et al., "qFibrosis: a fully-quantitative innovative method incorporating histological features to facilitate accurate fibrosis scoring in animal model and chronic hepatitis B patients," *J. Hepatol.* **61**(2), 260–269 (2014).
- R. M. A. Azzam, "Photopolarimetric measurement of the Mueller matrix by Fourier analysis of a single detected signal," *Opt. Lett.* **2**(6), 148–150 (1978).
- D. H. Goldstein, "Mueller matrix dual-rotating retarder polarimeter," *Appl. Opt.* **31**(31), 6676–6683 (1992).
- D. H. Goldstein and R. A. Chipman, "Error analysis of a Mueller matrix polarimeter," *J. Opt. Soc. Am. A* **7**(4), 693–700 (1990).
- D. B. Chenuault, J. L. Pezzaniti, and R. A. Chipman, "Mueller matrix algorithms," *Proc. SPIE* **1746**, 231–246 (1992).
- N. Ghosh, M. F. Wood, and I. A. Vitkin, "Mueller matrix decomposition for extraction of individual polarization parameters from complex turbid media exhibiting multiple scattering, optical activity, and linear birefringence," *J. Biomed. Opt.* **13**(4), 044036 (2008).
- E. Du et al., "Mueller matrix polarimetry for differentiating characteristic features of cancerous tissues," *J. Biomed. Opt.* **19**(7), 076013 (2014).
- M. Sun et al., "Characterizing the microstructures of biological tissues using Mueller matrix and transformed polarization parameters," *Biomed. Opt. Express* **5**(12), 4223–4234 (2014).
- M. Sun et al., "Probing microstructural information of anisotropic scattering media using rotation-independent polarization parameters," *Appl. Opt.* **53**(14), 2949–2955 (2014).
- C. He et al., "Characterizing microstructures of cancerous tissues using multispectral transformed Mueller matrix polarization parameters," *Biomed. Opt. Express* **6**(8), 2934–2945 (2015).
- V. Backman et al., "Detection of preinvasive cancer cells," *Nature* **406**(6791), 35–36 (2000).
- M. Dubreuil et al., "Mueller matrix polarimetry for improved liver fibrosis diagnosis," *Opt. Lett.* **37**(6), 1061–1063 (2012).
- T. Yun et al., "Monte Carlo simulation of polarized photon scattering in anisotropic media," *Opt. Express* **17**(19), 16590–16602 (2009).

Biographies for the authors are not available.